

# QUANTIFICATION OF THE AERODYNAMIC GAIN ON TWO VIRTUALLY COUPLED MODULAR TRAINS

SIWAR FADHEL & SAMUEL FROMONT  
Capgemini Engineering, Meudon, France.

## ABSTRACT

To make railway systems more autonomous and energy efficient, the suction phenomenon induced by virtual coupling (VC) can be considered as a beneficial source of energy saving since trains are very closely spaced. A minimum safe distance between railway systems must be defined and maintained to ensure the safety of the whole convoy. The purpose of this paper is to study and quantify the aerodynamic gain in case of VC of two modular and autonomous trains ‘Smart Cabins’ as designated in our project. Computational fluid dynamics simulations are investigated to analyze the aerodynamic effect under several scenarios by varying the inter-cabins distance. Some design simplifications have been made for each Smart Cabin to prepare simulations and reduce computation time. Simulation results confirm the interest of VC in the sense of reducing coefficient drag of the full convoy up to 27%, which reflects a power gain of about 4% of the total traction power required for a single Smart Cabin (~200 kW).

*Keywords: Aerodynamic, CFD, design, inter-cabin distance, virtual coupling.*

## 1 INTRODUCTION

An advanced approach of train control called virtual coupling (VC) has been recently proposed as an attractive technology for rail passenger and freight transport and for which driving fundamentals are similar to those of road platooning operation. In this driving mode, a safe distance must be kept between vehicles, which is much lower than the needed braking distance for the train’s full stop [1].

Many industrial projects and research studies are being carried out to define standards allowing the VC definition between railway systems. Standards will depend on the train type (freight/passenger: high speed, regional, metro, and tramway) and will specify many parameters: reference velocity, acceptable position and velocity uncertainties, minimum inter-vehicle distance, safety margin, Train-to-Train (T2T), Train-to-Infrastructure (T2I) communication delay, etc. Thus, new elements, such as sensors, control systems, T2T and T2I communication technologies, and VC management, in VC system must be defined.

Thanks to the recent advancement of wireless communication technology and signaling system [2]; in the future, trains will be able to share information continuously with neighbors and to receive reference signals from the VC infrastructure. One can refer to publications [1, 3, 4] and to MOVINGRAIL and X2RAIL projects deliverables under the Shif2Rail program [5, 6] to find out more about the VC concept.

The main purpose of a rail transport service is to satisfy travellers and freight customers’ requirements. Increasing the line capacity is one of the most important aspects that contributes to enhance user’s comfort. Therefore, an extensive state-of-the art has examined this aspect from different point of views like reducing user waiting times and rail failures systems. For example, authors in [7] define a new strategy that minimize user discomfort at different levels of degraded services. These studies define the problem of determining rail capacity as the maximum number of travelling trains. In this regard, VC would contribute to enhance the rail line capacity. In addition, VC reduces the headway and avoids expensive

railway infrastructure modifications by adding on-board electronic equipment on railway systems allowing trains coupling/decoupling dynamically. For example, trains leaving from the same station or travelling to the same destination can enter and leave the convoy in a versatile and a flexible manner. Another advantage of VC consists in reducing the coupling realization time. As widely shown in the literature [8, 9], the coupling/decoupling times have an influence on the cycle time of a railway service with direct repercussions on the maximum service frequency achievable on the line, therefore a real coupling could reduce the service frequency (and therefore of the line capacity) while a VC would make the frequency of service almost completely unchanged and thus maintain a good service performance. On the other hand, physical coupling only links trains with a same service type while VC provides the diversity of trains in the same railway platform by offering the possibility of connecting trains with different service types (people and goods).

In summary, VC state-of-the-art studies are more focused on defining required communications technology [10, 11], control systems [12, 13], and describing benefits only in terms of traffic and infrastructure without addressing the VC-added value in convoy energy efficiency. To the best of our knowledge, aerodynamic effects and energy savings have not been well addressed in the literature for railway systems; only one research work done by the same authors has been found [14, 15]. However, several investigations have been recently performed on platooning aerodynamic effects in automotive industry [16–23]. These studies confirm the potential of platooning in road transportation with regards to the overall convoy's aerodynamic drag reduction and fuel consumption.

In the scope of the Smart Train research project, this paper proposes a first simulation approach to prove the potential of VC in terms of energy saving. Simulations have been conducted based on a simple scenario composed of two identical Smart Cabins.

## 2 LITERATURE REVIEW AND MOTIVATION

In the early literature, many research works concerning aerodynamics have been developed in the automotive industry such as the ones in [24, 25]. Most of them have specially addressed the platooning for commercial vehicles. Recently, this concept has been more developed for road vehicles. Nevertheless, given the novelty of the concept in the railway industry, only one research work that has addressed the aerodynamic effects has been found [14, 15]. Typically, computational fluid dynamics (CFD) simulations are investigated in road industry to study the aerodynamic effects for platoon driving mode. Authors in [24] show that for a convoy formed by two buses at a cruising speed of 80 kph, there is an improvement of the drag coefficient  $C_D$  only for the leading bus if the inter-vehicle distance is less than 20 m, otherwise it is the following one that has the benefit. In [19], a platoon of two vehicles distanced by 10 m and driving at 80 kph produces a  $C_D$  reduction of 4% for the first and 40% for the second. As seen more recently in [22], simulations performed with two minibus and then two generic passenger cars show that the leading vehicle experienced a lower  $C_D$  compared to the following one and compared also to the isolated case. In addition, the following vehicle has a higher  $C_D$  than the isolated value. The case study of [14, 15] proves experimentally the VC benefit using the particle image velocimetry technique for all tested configurations with varying distance. Strong interaction is noticed for the smallest gap; up to 30% reduction of drag coefficient for the following train and up to 9% for the leading one in comparison to single train.

After the literature review, it is still difficult to understand the aerodynamic interest of the VC of two modular trains for individual entity and for the full convoy and to predict the

aerodynamic behavior of our Smart Cabin design in a platoon configuration, which we therefore aim to study and analyze.

### 2.1 Initial hypothesis

The VC positive effect on the Smart Cabin energy efficiency is mainly due to longitudinal forces influencing its dynamic motion. To obtain a mathematical model expressing the energy gain as a function of the aerodynamic gain, we have theoretically considered that VC can have a positive impact on drag coefficient not only on the following Smart Cabin but also on the leading one but with a minor importance. Authors in [18] and [20] have oriented their studies based on aerodynamic gain model expressed in [24]. To our knowledge, it was the only model reported in recent publications that expresses the drag coefficient gain as a function of inter-vehicle distance.

### 2.2 Longitudinal efforts modelling

Equation (1) establishes the Newton’s second law for longitudinal forces (i.e. x-component of forces) applied to a Smart Train composed of two Smart Cabins (Fig. 1), where the index  $i = 1,2$  corresponds to the  $i$ th cabin.

$$m_i a_i = F_{p,i} + F_{d,i} + F_{b,i} + F_{gx,i} + F_{r,i} \tag{1}$$

Where:

$m_i$ : mass of the train,  $a_i$ : train acceleration,  $F_{p,i}$ : propulsion force,  $F_{d,i}$ : aerodynamic drag force,  $F_{b,i}$ : braking force,  $F_{gx,i}$ : gravitational force, and  $F_{r,i}$ : rolling resistance force.

To simplify the modelling approach, we consider that  $m_1 = m_2$  and that both cabins have the same inclination angle, which leads to  $F_{gx,1} = F_{gx,2}$ ; moreover, we assume that they have

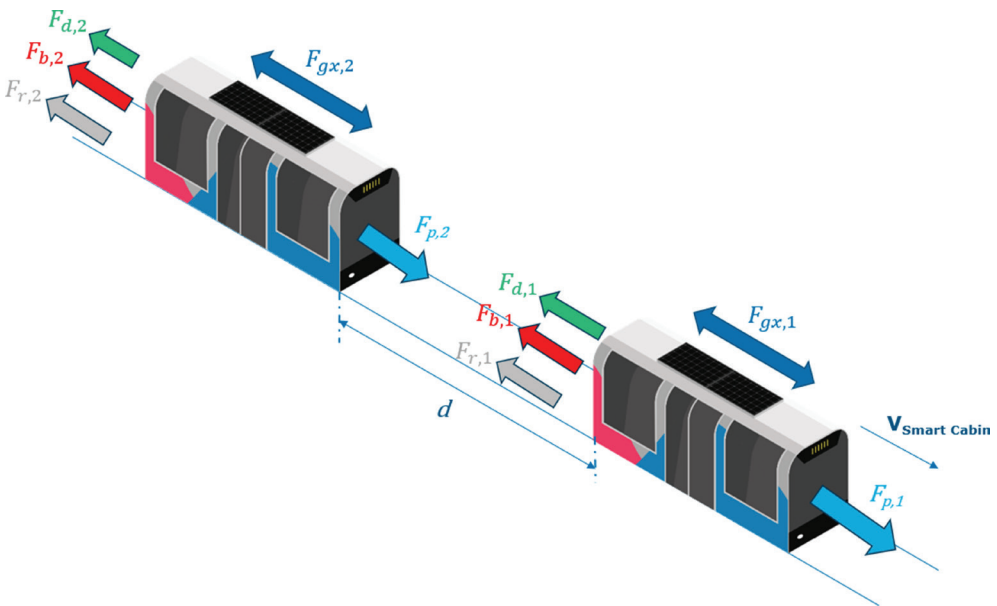


Figure 1: Longitudinal forces balance affecting the Smart Train motion.

the same braking efficiencies and rolling resistance coefficients, thus we have  $F_{b,1} = F_{b,2}$  and  $F_{r,1} = F_{r,2}$ .

As a result of these established equalities and considering that the acceleration  $a_i$  is the same for both cabins, only drag forces and therefore the propulsion forces are specific to each Smart Cabin in eqn (1).

### 2.3 Mathematical modelling of power and energy gain

The eqn (2) shows the expression of the drag reduction coefficient  $\Phi_2$  of the second vehicle introduced in [20], such an expression should be determined for the leading train coefficient  $\Phi_1$ . Equations (3) and (4) are the leading and the following train's drag force expressions, respectively.

$$\Phi_2(d) = \left( 1 - \frac{C_{D,1}}{C_{D,2} + d} \right) \tag{2}$$

$$F_{d,1} = \frac{1}{2} \Phi_1(d) C_d A \rho V^2 \tag{leading train} \tag{3}$$

$$F_{d,2} = \frac{1}{2} \Phi_2(d) C_d A \rho V^2 \tag{following train} \tag{4}$$

Based on the hypotheses exposed in 2.2, the eqn (5) expresses the difference of both trains' propulsion forces.

$$\Delta F_{p_{1 \rightarrow 2}} = F_{p,1} - F_{p,2} = F_{d,1} - F_{d,2} = \frac{1}{2} \left( \Phi_1(d) + \frac{C_{D,1}}{C_{D,2} + d} - 1 \right) C_d A \rho V^2 \tag{5}$$

The eqn (6) is a reminder of the relation between power, force, and velocity leading to the eqn (7), which is the difference of trains' propulsion powers that can be a gain for the following train if positive or a loss if negative.

$$\Delta P(W) = \Delta F.V \tag{6}$$

$$\Delta P_{1 \rightarrow 2} = \frac{1}{2} \left( \Phi_1(d) + \frac{C_{D,1}}{C_{D,2} + d} - 1 \right) C_d A \rho V^3 \tag{7}$$

To get the energy saving or loss for the following train, one needs to integrate over time eqns (6) and (7), which gives eqns (8) and (9), respectively.

$$\Delta E_c (J) = \int_0^t \Delta P . dt = \Delta P . t \tag{8}$$

$$\Delta E_{c_{1 \rightarrow 2}} = \frac{1}{2} \left( \Phi_1(d) + \frac{C_{D,1}}{C_{D,2} + d} - 1 \right) C_d A \rho V^3 . t \tag{9}$$

### 3 VC SIMULATION RESULTS

#### 3.1 Smart Cabin geometry and polyvalent service

In the context of Smart Train project, it is desired to offer an on-demand polyvalent service to transport passengers or/and micro-freights based on autonomous Smart Cabins that have an identical design. It should be noted that each Smart Cabin has a symmetrical external geometry for both services (people and goods), only the interior design will be rearranged to be adapted to the user's demand.

As shown in Fig. 2, the length  $L$  of the cabin is 12 m, the width  $l$  is 2.55 m, the height  $H$  without wheels is 3.09 m, and the corresponding frontal area is  $7.88 \text{ m}^2$ .

#### 3.2 CFD simulation setup

In this study, the aerodynamic performance of VC with two identical Smart Cabin geometries is analyzed using ANSYS FLUENT. The overall methodology is presented on Fig. 3.

First, design simplifications were performed on the initial geometry to limit the CAD size and the computational power required to generate the mesh. Second, preliminary evaluations were conducted on a single design to validate the appropriate mesh size and to determine its aerodynamic performance. Next, platoon simulations were performed for three different inter-vehicles distances. Finally, aerodynamic effects were analyzed based on drag coefficients obtained from CFD.

#### 3.3 Computational domain

For the Smart Train project, only the shuttle external geometry was used for the CFD simulation. We can see in Fig. 4, the CAD before and after the simplification and the preparation for simulation. The design version with two axles, one at the front and one at the rear, was chosen to simplify computations compared to the version with three axles at the front and three at the rear.

Furthermore, some elements and details have been suppressed, e.g. openings such as doors and windows have been closed. Also, the station platform and the ramp used for people with reduced mobility and rails are omitted (Fig. 4b).

Due to the symmetry of the shuttle external part, simulations were performed only on half of the geometry (Fig. 6c).

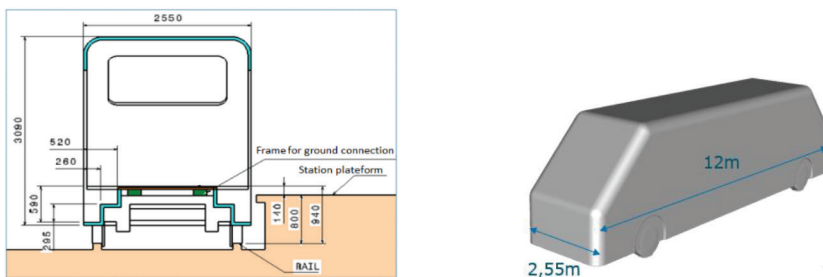


Figure 2: Smart Cabin dimensions.

Figure 5 shows the computational domain with a single cabin where the vein was extruded by a distance of  $2*L$  up front and  $4*L$  at the back of the cabin. The distance between the cabin and the vein side wall is equal to  $5*I$  and the distance between the cabin and the vein top wall is equal to  $6*H$ . In order to limit the size of the model and consequently the required computational time to carry out the simulation, three refinement boxes have been defined (see Fig. 6) corresponding to three mesh zones. The finest mesh box extensions are  $0.08*L$  at the front of the cabin,  $0.5*L$  at the back,  $0.39*I$  on the side, and  $0.65*H$  above the cabin. The remaining dimensions related to the intermediate and largest mesh boxes are indicated with blue and green arrows, respectively.

To characterize the aerodynamic performance of a single cabin, the physical parameters listed in Table 1 were specified and five different boundary conditions regions were defined as shown in Fig. 7.

### 3.4 Single Smart Cabin results

Figure 8a shows the skin friction coefficient contour on an isolated Smart Cabin. It highlights regions that mainly contribute to the aerodynamic drag force and thus to the drag coefficient. The critical areas where the flow is strongly accelerated correspond to the front and the rear faces.

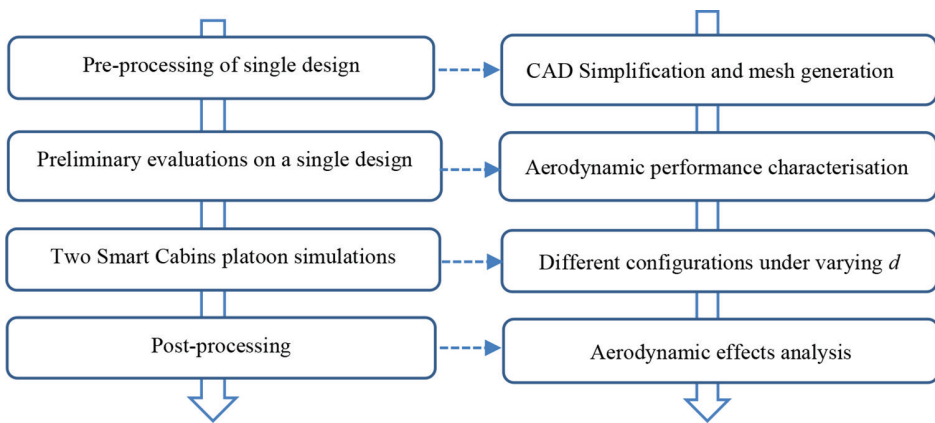


Figure 3: Flowchart of the CFD analysis methodology.

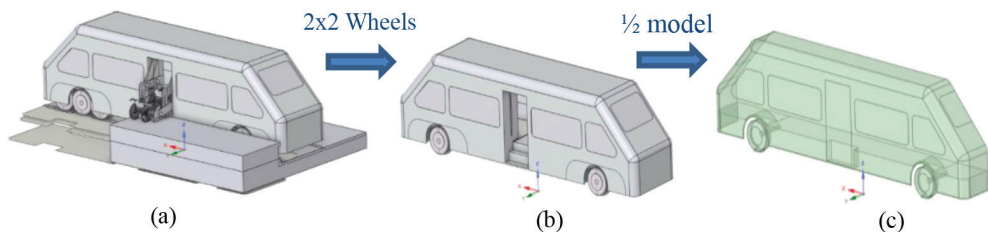


Figure 4: CAD simplification steps.

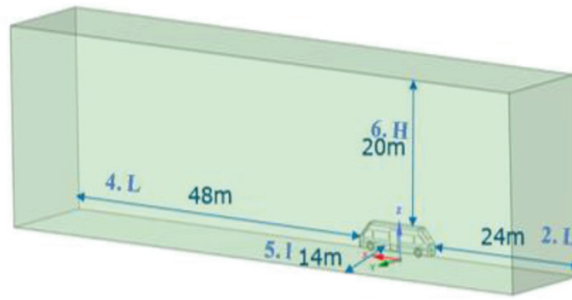


Figure 5: Computational domain (vein).

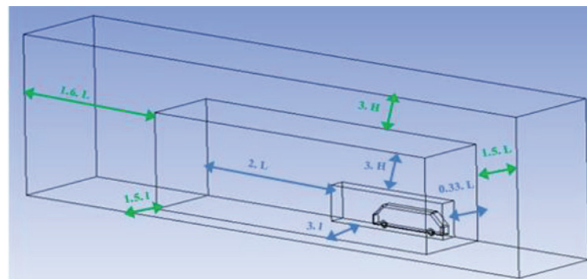


Figure 6: Refinement boxes.

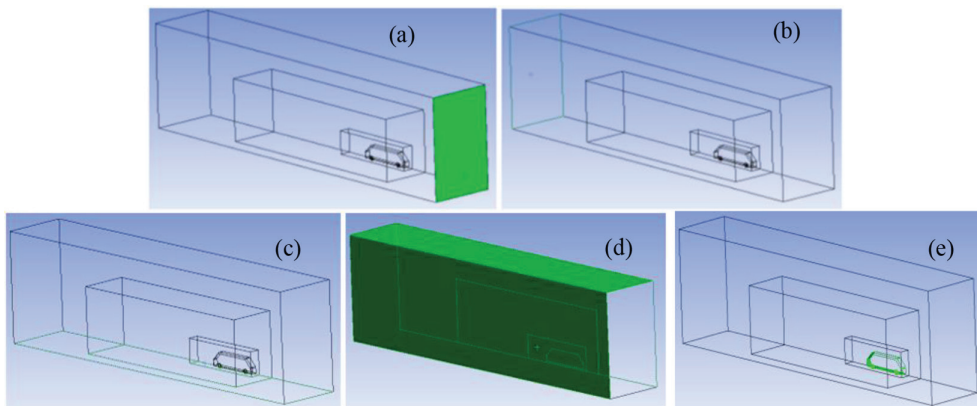


Figure 7: Boundary conditions regions: velocity inlet (a), pressure outlet (b), ground/wall (c), symmetry walls (d), and Smart Cabin/wall (e).

To ensure a correct value for the drag coefficient  $C_d$ , a convergence stopping criteria of  $1e-5$  was set and the convergence was reached after 3523 iterations (Fig. 8b). The last 100 iterations were used to calculate the  $C_d$  mean value which was equal to 0.46 and the aerodynamic drag force value  $F_d$  was 1089 N. It was calculated using the shuttle speed, its frontal area and the measured drag coefficient as shown previously in eqn (3).

Table 1: Boundary conditions parameters values.

Parameter	Value
Velocity	80 kph
Temperature	15°C
Air density	1.225 kg/m <sup>3</sup>
Air viscosity	1.7894e-5 kg/ms

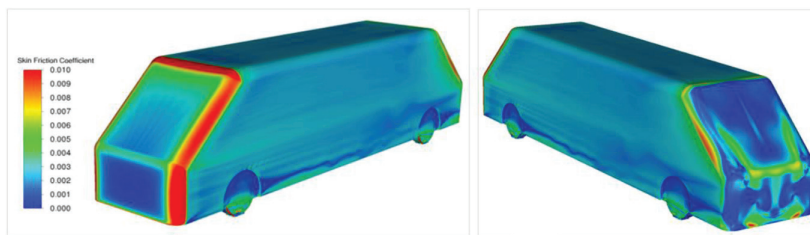


Figure 8: (a) Skin friction coefficient contour for a single Smart Cabin.

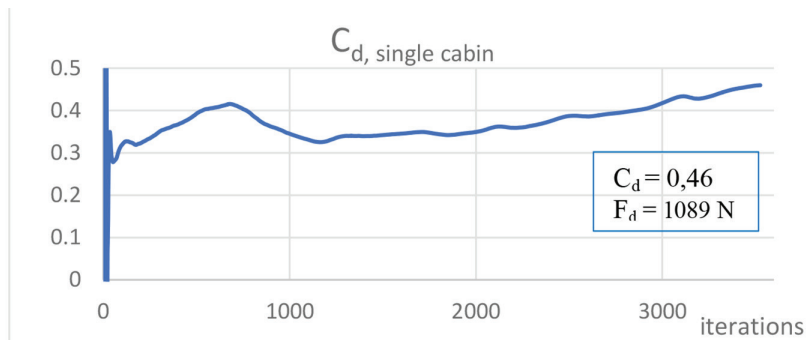


Figure 8: (b) Evolution of drag coefficient for a single Smart Cabin.

### 3.5 Virtually coupled Smart Cabins results

CFD simulations were carried out for three platoon configurations with a distance of 1, 5, and 10 m between the leading shuttle (Cabin 1) and the following shuttle (Cabin 2).

The three models with the corresponding drag coefficients result for both Cabin 1 and Cabin 2 are presented in Fig. 9. It should be noted that, for each configuration, the computational domain length was extended by the inter-cabins distance compared to the initial single cabin vein. The same distance  $4*L$  was kept between the following cabin and the vein outlet wall while keeping the leading cabin positioned at  $2*L$  from the vein inlet face.

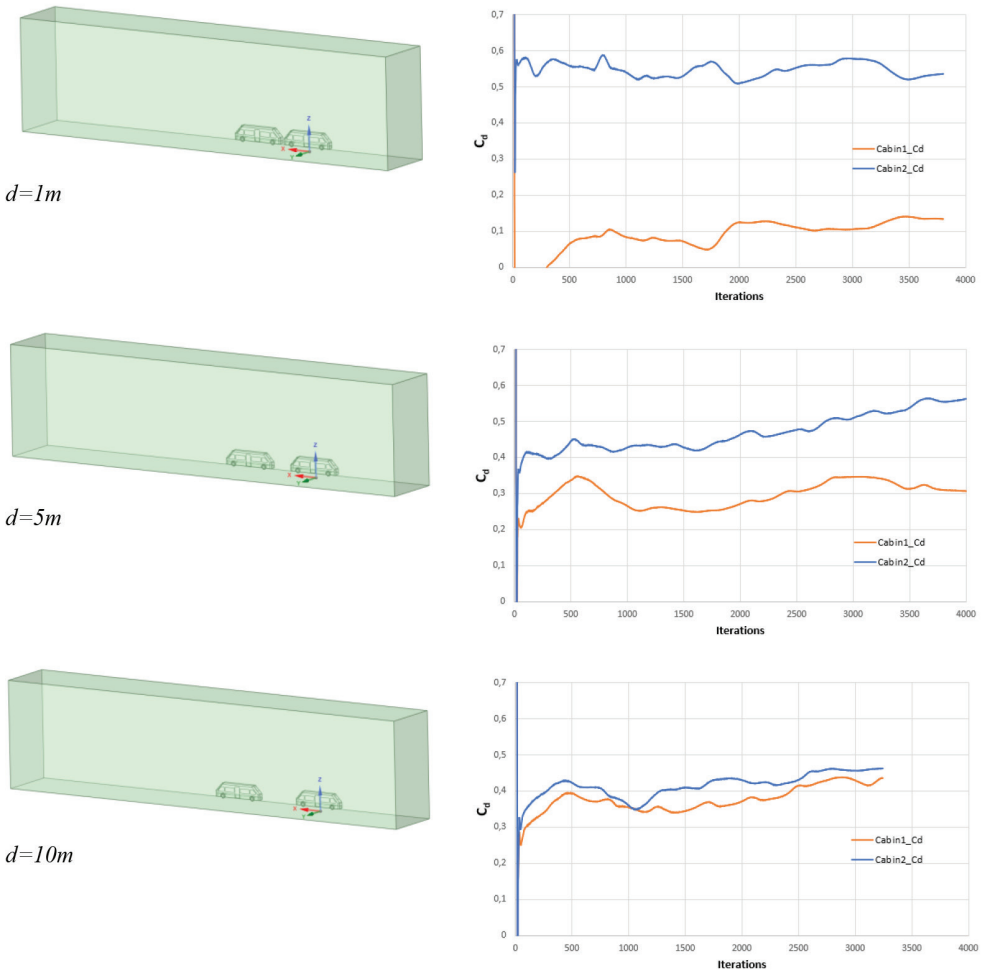


Figure 9: CFD simulations of the drag coefficient for the leading and following Cabin.

Simulation results showed a reduction of the platoon average drag coefficient ( $C_{d,platoon}$ ) of 26.81%, 5.23%, and 2.66% for  $d = 1$  m,  $d = 5$  m, and  $d = 10$  m, respectively (Table 2). Starting from  $d = 10$  m, the drag coefficient improvement becomes less significant. So, we can conclude that the aerodynamic benefit of the convoy using VC reduces as the inter-cabin distance increases.

We note that the leading Cabin experienced a lower drag coefficient  $C_{d,Cabin1}$  compared to the following Cabin 2's drag coefficient  $C_{d,Cabin2}$ . Moreover, we can see that  $C_{d,Cabin2}$  exceeds the isolated cabin  $C_{d,Cabin}$  for the three inter-cabin distances.

For better explanation of the shuttle's aerodynamic interaction for different platoon configurations, the cumulative  $C_d$  was plotted along the Smart Cabins bodies in Fig. 10. If we compare the single cabin case to cases with the inter-cabin distances of 1 and 5 m, we can conclude that:

Table 2: Drag coefficient values under different platoon distance at a velocity of 80 kph.

Simulated values	Simulation configurations			
	Single Smart Cabin	d = 1 m	d = 5 m	d = 10 m
$C_{d,1}$	0.46	0.13	0.31	0.43
$C_{d,2}$	0.46	0.53	0.56	0.46
$\langle C_{d,platoon} \rangle$	0.46	0.33	0.43	0.44
$\langle C_{d,platoon} \rangle_{reduction}$	-	26.81%	5.23%	2.66%

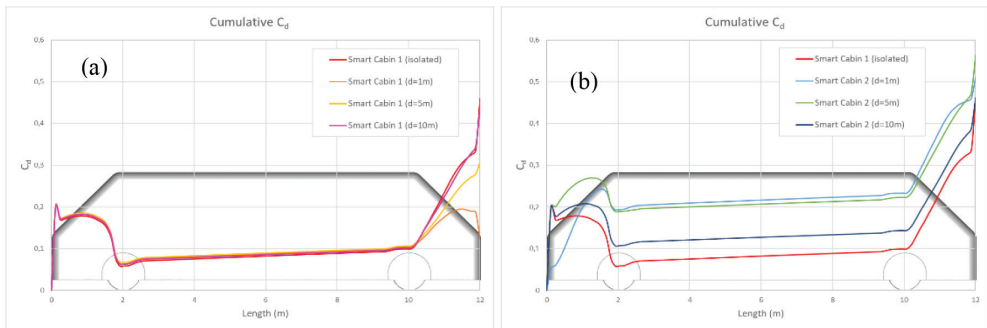


Figure 10: Comparison of the cumulative  $C_x$  on the design of the leading (a) and the following (b).

- the drag coefficient at the back of the leading cabin decreases when the distance  $d$  decreases,
- the drag coefficient at the front of the following cabin increases when the distance  $d$  increases.

For distance exceeding 5 m, the  $C_d$  values start to asymptotically converge towards the isolated value (Fig. 11). Consequently, to get aerodynamic benefit from platooning with the Smart Cabin design, shuttles must be separated by a distance located between 1 and 5 m.

### 3.6 Power gain analysis

The aerodynamic drag forces summarized in Table 3 were calculated based on eqns (3) and (4) with the measured drag coefficients of Table 2. The leading cabin drag force  $F_{d,1}$  is positively impacted, and the maximum power gain is reached in the case of a separating distance of 1 m. However, we note that the drag force of the following cabin  $F_{d,2}$  is above the single Smart Cabin value for the three platoon configurations and that both  $F_{d,1}$  and  $F_{d,2}$  converge towards it.

The platoon power gain is quantified based on assumptions made in 2.2 and represented by eqn (6), in our case since we have directly measured drag coefficients it is simply obtained by multiplying the drag forces difference with the cabins' velocity.

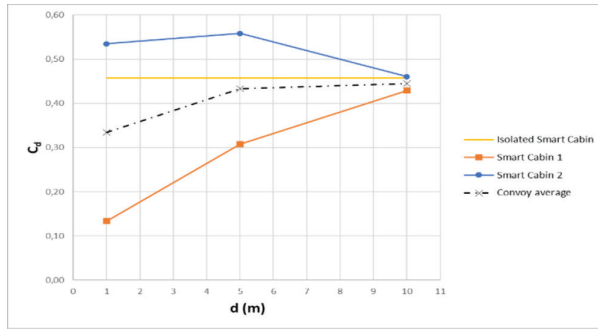


Figure 11: Drag coefficients convergence towards the isolated Smart Cabin value at  $d = 10$  m.

Table 3: Aerodynamic drag forces and power gain quantification.

Simulated values	Simulation configurations			
	Single Smart Cabin	$d = 1$ m	$d = 5$ m	$d = 10$ m
$F_{d,1}$ (N)	1089	318	735	1022
$F_{d,2}$ (N)	1089	1275	1330	1098
$\langle F_{d,platoon} \rangle$ (N)	1089	797	1032	1060
$\langle \Delta P_l \rangle$ (kW)	-	17.13	7.87	1.49
$\langle \Delta P_{platoon} \rangle$ (kW)	-	6.48	1.27	0.64
$\langle \Delta P_{platoon} \rangle_{gain}$	-	3.38 %	0.66%	0.33%

We have summarized in Table 3 the power reduction with respect to the power traction of one Smart Cabin. The most significant gain is achieved with an inter-cabin distance of 1 m. These results confirm that the optimized inter-cabin distance must be set between 1 and 5 m to make the most of the VC in terms of energy consumption.

### 3.7 Discussion and perspectives

CFD results performed on a platoon composed of two Smart Cabins show good agreement with literature results presented in [22]. In the present paper, we prove that the initial hypothesis based on an important gain for the following vehicle and a lesser one for the leading vehicle is not valid for our design with a platoon size of 2. However, we are not sure if it may be applicable for a greater number of Smart Cabins. Therefore, the present study opens several research questionings that will be answered in future works.

First, it would be very interesting to extend the study to multi-Smart Cabins platoons for the purpose of establishing a complete equation model of the air drag reduction as a function of the inter-cabin distance.

Second, studies could be done to define if there is a limit in convoy size when the VC becomes less aerodynamically beneficial and to calculate the optimized distance for this scenario.

#### 4 CONCLUSION

The work in this paper has established a preliminary basis that enabled us to study the platoon driving mode's aerodynamic benefit for the Smart Train using the VC technology. Simulations performed on a two-cabin convoy have shown the trend in drag coefficient change and corresponding power gain with the biggest one obtained with an inter-cabin distance of 1 m. Before studying models with larger platoons, additional calculations must be completed on the two-cabin convoy to precisely determine the inter-cabin distance value to get an optimized power gain. Also, the asymptotic value above which no significant reduction in drag coefficient is observed should be identified. Moreover, a mesh sensitivity study should be conducted with the aim of reducing models' size and thus computational time with polyhedral mesh for instance. This later work is essential to perform CFD simulations on convoys composed of more than two cabins. Then, a velocity sensitivity study could be realized to evaluate the drag coefficient variation with the cabin velocity set in the CFD simulations. Once all these sensitivity studies are done, the analysis work with a larger number of shuttles could be initiated. At a later stage, a valuable thing to do would be to calculate the energy savings of a platoon during a real driving cycle.

#### REFERENCES

- [1] Di Meo, C., Di Vaio, M., Flammini, F., Nardone, R., Santini, S. & Vittorini, V., ERTMS/ETCS virtual coupling: Proof of concept and numerical analysis. *IEEE Transactions on Intelligent Transportation Systems*, **21**(6), pp. 2545–2556, 2019. <https://doi.org/10.1109/tits.2019.2920290>
- [2] Unterhuber, P., *et al.*, A survey of channel measurements and models for current and future railway communication systems. *Mobile Information Systems*, **2016**, 2016.
- [3] Pan, J., Peng, Q., Zhan, S. & Bai, J., Multiscenario-based train headway analysis under virtual coupling system. *Journal of Advanced Transportation*, **2021**, 2021.
- [4] Aoun, J., Quaglietta, E., Rob, M. & Goverde, P., Investigating market potentials and operational scenarios of virtual coupling railway signaling. *Transportation Research Board*, **2674**(8), pp. 799–812, 2020. <https://doi.org/10.1177/0361198120925074>
- [5] MOving block and Virtual coupling New Generations of RAIL signalling [https://projects.shift2rail.org/s2r\\_ip2\\_n.aspx?p=MOVINGRAIL](https://projects.shift2rail.org/s2r_ip2_n.aspx?p=MOVINGRAIL). Accessed on: 21 Dec. 2020.
- [6] X2RAIL-3: [https://projects.shift2rail.org/s2r\\_ip2\\_n.aspx?p=X2RAIL-3](https://projects.shift2rail.org/s2r_ip2_n.aspx?p=X2RAIL-3) Accessed on: 23 Nov. 2020.
- [7] D'Acerno, L., Gallo, M., Montella, B. & Placido, A., Analysis of the interaction between travel demand and rail capacity constraints. *WIT Transactions on the Built Environment*, **128**, pp. 197–207, 2012.
- [8] D'Acerno, L. & Botte, M., Optimising frequency-based railway services with a limited fleet endowment: An energy-efficient perspective. *Energies*, **13**(10), Art. No. 2403, pp. 1–26, 2020. <https://doi.org/10.3390/en13102403>
- [9] D'Acerno, L. & Botte, M., Railway system design by adopting the Merry-Go-Round (MGR) paradigm. *Sustainability*, **13**(4), Art. No. 2033, pp. 1–21, 2021.
- [10] Unterhuber, P., Pfletschinger, S., Sand, S., Soliman, M., Jost, T., Arriola, A., Val, I., Cruces, C., Moreno, J., García-Nieto, J. P., Rodríguez, C., Berbineau, M., Echeverría, E. & Baz, I., A survey of channel measurements and models for current and future railway communication systems. *Mobile Information Systems*, pp. 1–14, 2016.
- [11] Stickel, S., Schenker, M., Dittus, H., *et al.*, Technical feasibility analysis and introduction strategy of the virtually coupled train set concept. *Scientific Reports*, **12**, p. 4248, 2022. <https://doi.org/10.1038/s41598-022-08215-y>

- [12] Cao, Y., Wen, J. & Ma, L., Tracking and collision avoidance of virtual coupling train control system. *Future Generation Computer Systems*, **120**, pp. 76–90, 2021. <https://doi.org/10.1016/j.future.2021.02.014>
- [13] Felez, J., Kim, Y. & Borrelli, F., A model predictive control approach for virtual coupling in railways. *IEEE Transactions on Intelligent Transportation Systems*, **29(7)**, pp. 2728–2739, 2019.
- [14] Wilhelmi, H., Thieme, T., Henning, A. & Wagner, C., Aerodynamic investigations of the effects of virtual coupling on two next generation trains. *New Results in Numerical and Experimental Fluid Mechanics XI, Contributions to the 20th STAB/DGLR Symposium. Notes on Numerical Fluid Mechanics and Multidisciplinary Design*, Springer, Cham, pp. 695–704, 2018.
- [15] Thieme, T., Wilhelmi, H., Henning, A. & Wagner, C., Force and flow measurements on two trains in Platoon Configuration. *3rd International Symposium on RAIL AERODYNAMICS*, Germany, 2018.
- [16] Lammert, M. P., Duran, A., Diez, J., Burton, K. & Nicholson, A., Effect of platooning on fuel consumption of Class 8 vehicles over a range of speeds, following distances, and mass. *SAE Int. J. Commercial Vehicles*, **7(2)**, pp. 626–639, 2014. <https://doi.org/10.4271/2014-01-2438>
- [17] Alam, A., Mårtensson, J. & Johansson, K. H., Experimental evaluation of decentralized cooperative cruise control for heavy duty vehicle platooning. *Control Engineering Practice*, **38**, pp. 11–25, 2015. <https://doi.org/10.1016/j.conengprac.2014.12.009>
- [18] Torabi, S. & Wahde, M., Fuel-efficient driving strategies for heavy-duty vehicles: A platooning approach based on speed profile optimization. *Journal of Advanced Transportation*, **2018**, pp. 1–12, 2018. <https://doi.org/10.1155/2018/4290763>
- [19] Norrby, D., *A CFD study of the aerodynamic effects of platooning*. KTH Royal Institute of Technology, Stockholm, Sweden, 2014.
- [20] Turri, V., Besselink, B. & Johansson, K. H., Cooperative look-ahead control for fuel-efficient and safe heavy-duty vehicle platooning. *IEEE Transactions on Control Systems Technology*, **25(1)**, pp. 12–28, 2017. <https://doi.org/10.1109/tcst.2016.2542044>
- [21] Turri, V., *Look-ahead control for fuel-efficient and safe heavy-duty vehicle platooning*, KTH Royal Institute of Technology, Stockholm, Sweden, 2018.
- [22] Teja Kaluva, S., Pathak, A. & Ongel, A., Aerodynamic drag analysis of autonomous electric vehicle platoons. *Energies*, pp. 1–18, 2020.
- [23] Cerutti José, J., Sardu, C., Cafiero, G. & Iuso, G., Active flow control on a square-back road vehicle. *Fluids*, pp. 1–27, 2020.
- [24] Hucho, W.-H., *Aerodynamics of Road Vehicles*. Oxford, UK: Butterworth–Heinemann, 1987.
- [25] Zabat, M., Stabile, N., Farascaroli, S. & Browand, F., *The aerodynamic performance of Platoons: A Final Report*. California Partners of Advanced Transit and Highways (PATH), Institute of Transportation Studies, University of California, Berkeley, 1995.